POLITECNICO DI TORINO
Repository ISTITUZIONALE

Prediction and validation of fire parameters for a selfextinguishing and smoke suppressant electrospun PVPbased multilayer material through machine learning models

Original
Prediction and validation of fire parameters for a selfextinguishing and smoke suppressant electrospun PVPbased multilayer material through machine learning models / Bifulco, A., Climaco, I., Casciello, A., Passaro, J., Battegazzore, D., Nebbioso, V., Russo, P., Imparato, C., Aronne, A., Malucelli, G.. - In: JOURNAL OF MATERIALS SCIENCE. - ISSN 1573-4803. - ELETTRONICO. - 60:(2025), pp. 1019-1040. [10.1007/s10853-024-10529-3]

Availability:
This version is available at: 11583/2996413 since: 2025-01-09T10:12:47Z

Publisher:
Springer

Published
DOI:10.1007/s10853-024-10529-3

Terms of use:

This article is made available under terms and conditions as specified in the corresponding bibliographic description in the repository

Publisher copyright

(Article begins on next page)

31 October 2026

J Mater Sci (2025) 60:1019–1040

Polymers & biopolymers

Prediction and validation of fire parameters for a self-extinguishing and smoke suppressant electrospun PVP-based multilayer material through machine learning models

Aurelio Bifulco[1,*], Immacolata Climaco[1], Angelo Casciello[1], Jessica Passaro[2], Daniele Battegazzore[3], Viviana Nebbioso[1], Pietro Russo[2], Claudio Imparato[1], Antonio Aronne[1], and Giulio Malucelli[3]

[1] *Department of Chemical, Materials and Production Engineering (DICMaPI), University of Naples Federico II, P.le Tecchio 80, 80125 Naples, Italy*

[2] *Institute for Polymers, Composites and Biomaterials-National Council of Research, Via Campi Flegrei 34, 80078 Pozzuoli, Naples, Italy*

[3] *Department of Applied Science and Technology, Politecnico di Torino, Viale Teresa Michel 5, 15121 Alessandria, Italy*

Received: 26 September 2024
Accepted: 4 December 2024
Published online: 28 December 2024

© The Author(s), 2024

ABSTRACT

Electrospinning is a technology largely employed to obtain polymer fibers with different functionalities. The electrospinning of polyvinylpyrrolidone (PVP) in the presence of silica nanoparticles, and the subsequent thermal treatment of these electrospun PVP-silica fibers, allows for the manufacturing of a self-extinguishing material stable in polar solvents. However, this material lacks consistency and does not sustain any load: this strongly limits its application in many industrial fields (e.g., the aerospace sector). Herein, we used cross-linked electrospun PVP-silica blankets and TiO_2 nanoparticles to coat hemp blankets, producing a multilayer material (MM) by surface charge interaction. The MM exhibited lower stiffness than the original hemp fabric but still good mechanical behavior, V0 class at the UL 94 vertical burning test, and good stretchability even after direct flame exposure. Further, burn-through and cone calorimetry tests revealed that MM is an excellent smoke suppressant and fireproof fabric, with very low total smoke release values (as low as 4.9 vs. − 33.3 m^2/m^2 measured for hemp) and its structure remained intact for at least − 1 min. Finally, as all the aforementioned experimental activity, though necessary and unsubstantial, is usually quite time-consuming, two Machine Learning models were developed and exploited to predict the fire performances related to the multilayer material. Despite the incomplete starting datasets, the implemented models accounted for a successful prediction of the target parameters (namely, Time to Ignition and peak of Heat Release Rate),

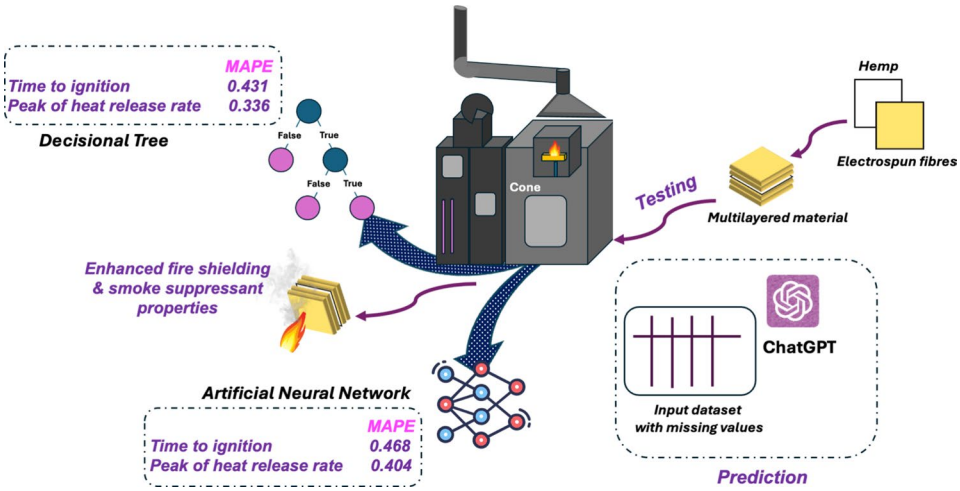
Handling Editor: Jaime Grunlan.

Address correspondence to E-mail: aurelio.bifulco@unina.it

https://doi.org/10.1007/s10853-024-10529-3

thanks to the assistance of ChatGPT and the exploitation of made-on-purpose decision trees.

GRAPHICAL ABSTRACT



Introduction

Electrospinning is a well-known technology for manufacturing polymer nanofibers with multiple architectures [1, 2]. The wide application of such methodology is mainly due to its capability to produce micro/nanofibers ranging from 2 nm to several micrometers, while conventional processes only allow for the fabrication of larger continuous fibers. Owing to these peculiarities, electrospinning is frequently applied in medical areas (e.g., tissue engineering), where nanofibers exhibiting specific electronic and photocatalytic properties are highly desired [1, 3, 4]. On the other side, recently, the demand for electron nanofibers with excellent thermal behavior, flame retardancy, and mechanical response is increasing, as they can be employed to obtain multifunctional nanofibrous nonwovens, air filtration membranes, fire protective coatings, and reinforced polymeric composites [5–8]. However, many products based on polymer electrospun nanofibers, especially the ones produced starting from safe and sustainable poly(vinyl pyrrolidone) (PVP) and poly(vinyl alcohol) (PVA), do not show good mechanical properties, making them suitable as reinforcements but not as structural components [9, 10]. This issue can be overcome through the incorporation of solid particles into the polymer matrix: as a result, its mechanical performances, such as stiffness, toughness, and impact strength, improve [11–13]; however, in the case of micro/nanofibers the effectiveness of fillers in contrasting this issue is limited. PVP-based nanofibers can be used for the preparation of materials employed in medicine and other biological systems [14, 15], although the high PVP solubility in water strongly limits the application of its electrospun blankets, causing low durability at different operative conditions [16, 17]. To overcome this limitation, the crosslinking of electrospun polymeric nanofibers by thermal treatment is one of the most feasible possibilities [5, 18, 19], though it often leads to an unwanted shrinkage of the annealed samples. Newsome et al. demonstrated that the incorporation of sub-micrometer silica particles into electrospun PVP fibers can prevent the occurrence of shrinkage phenomena during their crosslinking by heat treatment at 200 °C, leading to high-quality water- and moisture-resistant composite fibers [20]. Following a similar procedure, Passaro et al. produced crosslinked silica/PVP electrospun composite fibers showing high water resistance and negligible shrinkage [19, 21].

In the context of sustainability, natural fibers such as kenaf, hemp, flax, and jute are becoming more and more crucial to developing greener fiber-reinforced polymeric composites, as their exploitation results in a remarkable reduction of weight, CO_2 release, and costs [22–24]. Among the natural fibers, hemp can be employed in several industrial applications; recent statistics confirm, for the U.S. market, an expected

value of USD 16.75 billion, with a compound annual growth rate of 17.1% from 2023 to 2030 [25]. One drawback related to the use of sustainable hemp fibers is their high flammability: thus, many chemical strategies have been developed to flame retard these fibers [26]. However, most of these methodologies consist of time-consuming procedures involving low sustainable nitrogen- and phosphorus-based compounds, causing high energy utilization and the depletion of natural resources [27, 28]. In this context, the deposition via sol–gel chemistry of blankets made of crosslinked silica/PVP electrospun composite fibers on hemp rugs may represent an effective, affordable, and timesaving approach to preparing self-extinguishing multilayer materials, without the use of any N- or P-based compounds.

For these reasons, in this work, we thoroughly investigated a multilayer material composed of hemp rugs coated using blankets made of crosslinked silica/PVP electrospun composite fibers. The adhesion between these materials was obtained by electrostatic interactions. An acidic solution containing titanium dioxide nanoparticles was employed along the process to tune the proper surface charge on the PVP-based blankets. We deeply investigated the fire behavior and flammability of the produced multilayer material, together with its mechanical response. The multilayer material kept the sustainable features of its components unchanged, but showed self-extinguishing capability, excellent smoke suppressant behavior, and very good mechanical strength, overcoming all the limitations of hemp rugs and PVP-based blankets.

Finally, to overcome the restraints related to the need to (1) perform a huge number of destructive tests and (2) synthesize and characterize several flame retardant formulations, aiming to design new effective flame retardant polymeric and textile materials, we developed and implemented two robust and reliable models through a Machine Learning (ML) approach, suitable for predicting two parameters (i.e., Time to Ignition and peak of Heat Release Rate, from forced-combustion tests) for the investigated electrospun PVP-based multilayer material. Artificial intelligence models, especially ML ones (e.g., artificial neural networks, decision trees) and metaheuristic algorithms (e.g., grey theory-white shark optimizer), are being increasingly applied in the predictive study and optimization of morphological, mechanical, viscoelastic, and functional (e.g., soundproofing) properties of new polymeric and textile products [29–32], overcoming the main limitations of numerical simulation models [33]. Some literature reports thoroughly discuss the application of ML models on different input data also for the prediction of thermal and fire performances of polymeric materials [34–37]. Indeed, ML is one of the most reliable predictive methods, as it does not involve any arbitrary assignment or the use of predetermined equations, but it learns information directly from data relying on algorithms (e.g., locally weighted regression algorithms) or computational systems [31, 38].

However, it frequently occurs that the available dataset, employed for building the machine learning model, shows several missing experimental values. This may negatively affect the accuracy of the neural network and thus the prediction. To overcome this issue, after a statistical evaluation of these datasets and their distributions, chat generative pre-trained transformer (ChatGPT), a chatbot developed by OpenAI, can replace the missing values with mean, mode, or median, and suggest the best ML model, suitable for the prediction of specific parameters [39–41]. This quite new strategy was recently demonstrated by Bifulco et al. [42] and Amor et al. [32, 43, 44].

Therefore, in this work, we aim to demonstrate that the integration of ChatGPT to perform a data improvement and the implementation of well-designed ML models allow for the prediction of fire behavior with satisfactory accuracy, even when some input data are missing. These findings may pave the way for the design and implementation of novel and reliable AI-based tools in materials science and technology, which, far from aiming to skip the always required experimental activity, can significantly help the researchers in reducing the time efforts, leading to the envisaged research objectives.

Materials and methods

Materials

Hemp (H) sheets, supplied by MAEKO S.r.l. (Milan, Italy), were used without any pretreatment. Tetraethyl orthosilicate (TEOS, > 99%), ammonium hydroxide (30–33% NH_3 in H_2O), ethanol (99.8%), polyvinylpyrrolidone (PVP, MW: 1300000 g mol^{-1}), purchased from Sigma-Aldrich (Merck KGaA, Darmstadt, Germany), were used to produce the PVP-silica blankets. Titanium dioxide nanoparticles (TiO_2 P90) from Evonik

(Hanau-Wolfgang, Germany), hydrochloric acid (37 wt.%), and acetic acid (98%) from Sigma-Aldrich were used for the preparation of the multilayer.

Manufacturing of the multilayer material

PVP-silica blankets were fabricated by electrospinning, following the same procedure previously reported [21]. The SiO_2 nanoparticles were prepared through the Stöber sol–gel method using TEOS as a precursor. A suspension (40 wt.%) of silica particles in ethanol was mixed with an ethanol solution (20 wt.%) of PVP. The resulting suspension was electrospun under a voltage of 30 kV at room temperature and a humidity of (45 ± 10)%, ensuring a flow rate of 0.100 mL min^{-1}. The electrospun non-woven mats were dried at 80 °C for 60 min, then slowly heat-treated from 150 to 200 °C, and finally kept for 6 h at 200 °C. Such thermal treatment makes the PVP matrix of the composite mats resistant to humidity, without significant shrinkage, thanks to the backbone of silica nanoparticles embedded into the fibers. Moreover, the sol–gel silica particles are partly exposed at the fibers' surface, which allows for their surface chemistry exploitation [21, 45].

The hemp/PVP-silica multilayer material was prepared favoring the adhesion between the blankets through electrostatic interaction, as in a layer-by-layer manufacturing approach. In a typical procedure, first, a single layer (5 × 5 × 0.1 cm^3) of hemp was soaked for 5 min in a water solution, acidified by using HCl, at pH 2.5, which is slightly higher than the isoelectric point (2.0–2.5) of silica nanoparticles, but lower than that of hemp (> 3.0) [46]. The deposition of one PVP-silica blanket (5 × 5 × 0.05 cm^3) was performed on each side of the hemp sample, assisted by electrostatic interaction. To improve the adhesion of blankets with hemp in the bilayered material (named H-2PVP), this was thermally treated in an oven for 1 h at 80 °C. H-2PVP was further coated by 4 layers of PVP-silica blankets on each side to improve its fire behavior (see Sect. "Mechanical robustness and flammability behavior of the multilayer material"). To obtain a good electrostatic interaction and thus a satisfactory adhesion between the PVP-silica blankets, H-2PVP was soaked for 5 min in a water suspension of TiO_2 nanoparticles (0.1 M), acidified by using acetic acid (at pH 5). Then, H-2PVP was kept in an oven for 1 h at 80 °C to support the condensation reactions between Si–OH and Ti–OH groups and ensure a neutral charge on the surface of the bilayered material. To create a positive charge on the surface of the thermally treated H-2PVP, 2 mL of the solution containing TiO_2 particles at pH 5 were uniformly distributed on its surface before laying a dried PVP-silica blanket, which is expected to become negatively charged at that pH value. To promote the electrostatic interaction and the adhesion of the PVP-silica blanket on the surface of H-2PVP, the blanket was roll-pressed with a glass rod, removing the excess solution, and then the sample was kept in an oven for 20 min at 80 °C. This procedure was repeated on the other side of H-2PVP and for further three times (a total of 10 PVP-silica layers) to obtain a multilayer material (named H-10PVP). Finally, H-10PVP underwent a thermal treatment at 80 °C for 1 h to achieve a dried sample that appeared completely different, when compared to the material assembled by the simple deposition of five PVP-silica blankets on each side of a hemp layer (named H-as10PVP). The whole procedure is schematized in Fig. 1A and the two multilayer samples are shown in Fig. 1B.

Experimental characterization

The **weight per unit area** was measured for hemp and H-10PVP multilayer samples by weighing a sample with a specific area of 25 cm^2. The following values were obtained: 234 g/m^2 for H and 428 g/m^2 for H-10PVP.

The **washing fastness** of multilayer material was evaluated by employing a solution containing 4 g/L of commercial detergent; the liquor ratio was 50:1. Each washing step was performed at 40 °C for 5 min. After each washing cycle, the fabric was removed, squeezed, and rinsed with tap water. Then, repeated washing was carried out until a total of 250 min was reached [46, 47].

The chemical analysis of the material was performed by **Fourier-transform infrared (FTIR) spectroscopy** in Attenuated Total Reflectance (ATR) mode, using a Nicolet 5700 spectrometer (ThermoFisher, Waltham, MA). The spectra were collected from 32 scans with a resolution of 4 cm^{-1}. The char samples produced after flame spread tests were also analyzed by ATR-FTIR spectroscopy.

The surface morphology and chemical composition of the prepared material and the residual char were examined using an EVO 15 **scanning electron microscope (SEM)** from Zeiss (Oberkochen, Germany), coupled with an Ultim Max 40 **energy-dispersive X-ray**

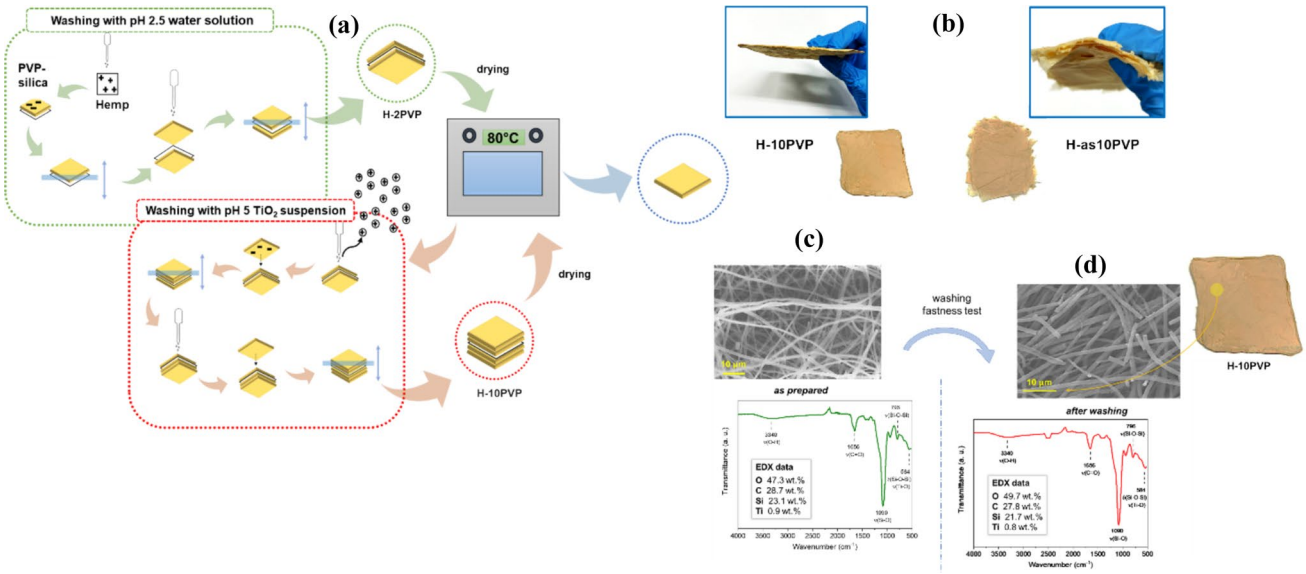


Figure 1 **a** Scheme of the fabrication procedure of hemp/PVP-silica bilayer (H-2PVP) and multilayer (H-10PVP) materials; **b** photographs of H-10PVP and H-as10PVP samples; **c** SEM image, ATR-FTIR spectrum and EDX elemental analysis results for H-10PVP; **d** SEM image, ATR-FTIR spectrum and EDX results for H-10PVP after laundry cycles.

(EDX) micro-analyzer (Oxford Instruments, High Wycombe, UK).

The thermal behavior of H-10PVP was studied by **thermogravimetric analysis (TGA)**, using a simultaneous thermoanalyser SDT Q600 (TA Instruments, New Castle, DE, USA) under N_2 and air with a gas flow of 100 mL/min, in the temperature range 25–800 °C at a heating rate of 10 °C/min.

The **flammability** of the multilayer material was investigated, like in the case of polymer-based composites, using the Underwriters Laboratories 94 (UL 94) vertical burning test, following the ASTM D3801 standard. The size of the test specimens was 125 × 13 × 3 mm^3 and the burning test was repeated until five consecutive readings.

Burn-through tests were performed on bare hemp and H-10PVP to evaluate their resistance toward the frontal application of a flame. A small-scale butane burner apparatus (Cadrim, China) was used to carry out the tests. The flame temperature was about 1200 °C and the generated front heat flux was around 170 kW/m^2. The temperatures at the backside of the specimens (10 × 10 cm^2) and related burn-through time and ignition time were monitored by an **InfraRed camera** Thermo Gear G100/G120 (NEC Avio Infrared Technologies Co., Tokyo, Japan). Details about the experimental setup and procedure are described in Figure S1 and in a previous work [48].

The fire behavior of bare hemp and multilayer blankets was evaluated by a **cone calorimeter** (Noselab ATS, Monza, Italy), operating with an irradiative heat flux of 35 kW/m^2 (ISO 5660 standard). The cone calorimetry tests were performed on 10 × 10 cm^2 specimens to determine the time to ignition (TTI, s), time to flame out (TTFO, s), total heat release (THR, MJ/m^2), heat release rate (HRR, kW/m^2), peak of the heat release rate (pkHRR, kW/m^2), total smoke release (TSR, m^2/m^2), specific extinction area (SEA, m^2/kg), carbon monoxide and carbon dioxide yields (kg/kg).

The **tensile properties** of the hemp fabric and H-10PVP were evaluated using an Instron Mod. 4505 dynamometer. Specifically, three rectangular strips for each type of sample, having a width of 30 mm and preliminarily conditioned at room temperature and 50% relative humidity for 2 days in a climatic chamber, were tested by setting a crosshead speed of 2 mm/min.

Machine learning modelling and design strategy

Cone calorimetry test is useful to deeply investigate the fire behavior of a flame retardant polymeric material. It is a disruptive test, which normally needs three specimens to provide reliable results. This forced-combustion test is performed in air atmosphere and the flaming combustion of volatiles,

generated by heat radiation, is triggered through a spark igniter. Among the possible fire parameters (see Sect. "Thermal and fire performances of the multilayer material"), which can be measured by cone calorimetry tests, TTI and pkHRR are particularly useful for fire scientists to study the effect of a specific flame retardant on a polymer-based material. These two parameters can also be evaluated by additive molar group contributions; however, both methods are time-consuming [49, 50]. Besides, the forced-combustion test is not only a disruptive measurement, but it also requires an expensive apparatus that is frequently not available in many research laboratories and companies. Recently, as an alternative to these approaches, some works have demonstrated that machine learning models enable the prediction of cone calorimetry parameters of many polymeric systems [42]. The application of machine learning (ML) models allows to avoid the use of time-consuming procedures and expensive instruments, reducing the number of measurements, and the loss of material during the screening operations in the design of experiments. However, in the prediction of materials' physico-chemical properties by machine learning, the lack of complete and large datasets is one of the major drawbacks. Most of the available and suitable datasets in the literature are characterized by a large presence of missing values, which makes it difficult to train efficient models [51].

Herein, by the application of KNIME, an open-source software for managing data science [52], we employed different machine learning models (i.e., artificial neural networks and decision trees) to predict the TTI and the pkHRR of the multilayer material (H-10PVP) from its weight per unit area, cone calorimetry parameters, TGA data, and vertical flame spread test results (see the input dataset in Table S1). The input parameters (IPs) for the models, together with their symbols and meanings, are listed in the rows and columns of Table S1. More in detail, the columns of the IPs are weights per unit area, cone calorimetry parameters, TGA data, and vertical flame spread test results of functionalized and neat textile materials (see column of references in Table S1), whose experimental values were found in the literature [53], including hemp, i.e., the material selected for this research work. H was taken into account to complete the input dataset, as it represents the true reference and counterpart of H-10PVP, therefore it is crucial to keep a high accuracy for the models.

The four stages performed in this study for the prediction of the cone calorimetry data (TTI and pkHRR) related to H-10PVP are reported in the workflow of Fig. 2. In the first stage, as above mentioned, the IPs dataset, for the machine learning models, is built by using laboratory measurements (see following sections), in the case of H and H-10PVP, and data found in the literature for the other textile materials. The second stage involves the execution of data pre-processing operations by generative model ChatGPT. As reported in Table S1, the IPs dataset shows some missing values; this aspect may reduce the predictive capability of the ML models. Considering the data distribution and statistical analysis, ChatGPT was employed to enhance the starting IPs dataset by replacing each missing value with the most suitable statistical indicator (i.e., mean, median or mode). In particular, the GPT-4 model was chosen among the various models provided by OpenAI, given its ability to take in input and process excel files, in which our data were stored. Before running ChatGPT, textile materials in Table S1 were grouped based on their chemical-physical similarity and a specific number (see "SAMPLE ID" column) was associated to each cluster. This preliminary clustering operation allows to (i) estimate more representative statistical indicators, as ChatGPT can work separately on small portions of data rather than on the whole dataset, and (ii) apply stratified sampling during model training, so training and validation datasets will have a similar number of samples for each group. To prevent negative effects along the training of the models, the new IPs dataset (Table S2), containing the statistical indicators found by ChatGPT, was further modified through the removal of nine rows and one column, as their missing values could not be obtained with the generative model. After this cleaning operation, the resulting IPs dataset (Table S3) was used (see Fig. 2) to determine the best regression models to be applied on the available data. Due to the low number of data, the input dataset was not submitted to features selection techniques (e.g., principal component analysis). Also, the data were not normalized to prevent any change of scale altering the significance of the parameters (i.e., chemical-physical properties of the textiles) and negatively influencing the training of the artificial neural networks (ANNs). There are several tools that can be employed to improve the quality of very wide input dataset, for example the methods based on cooperative game theories (e.g., Shapley Additive Explanations). These methods allow for increasing

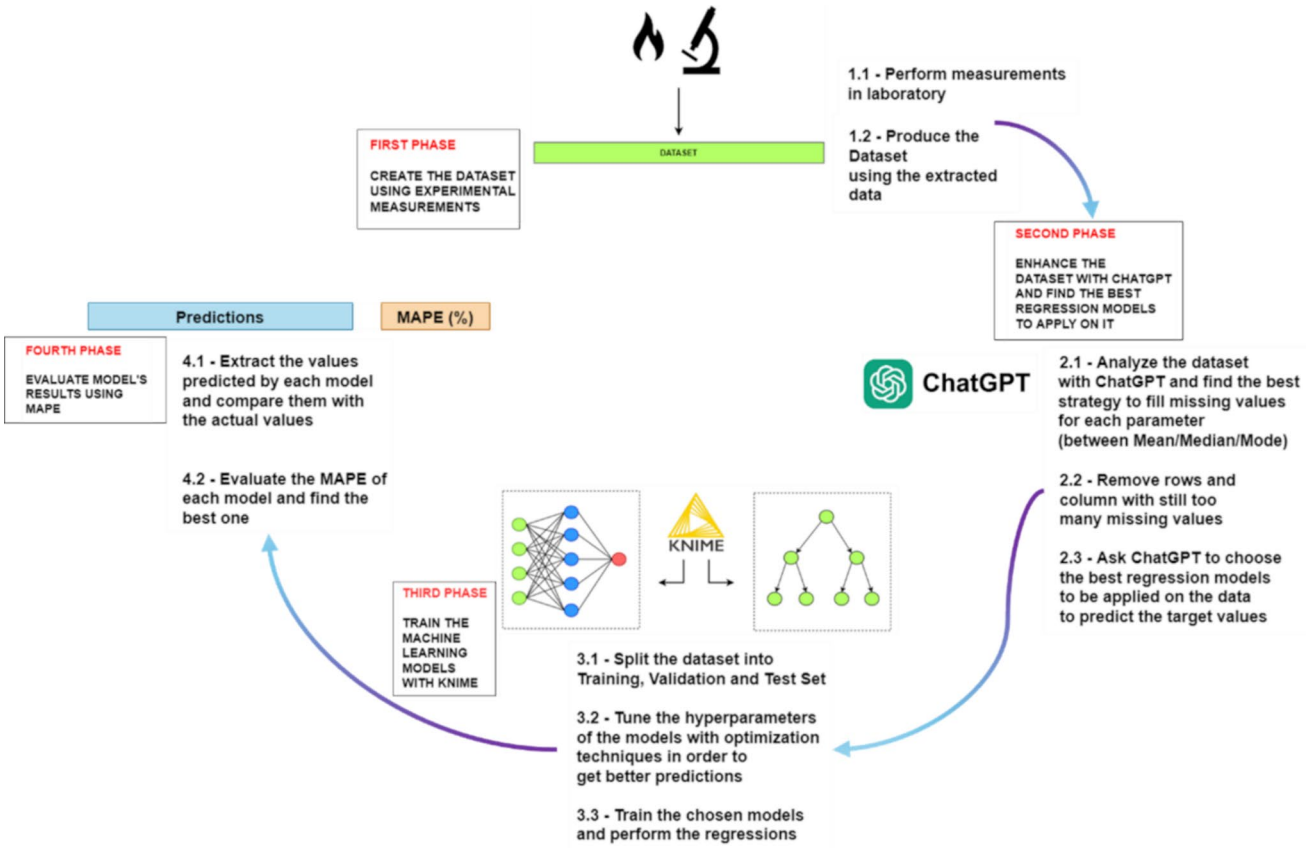


Figure 2 Workflow reporting the four stages used to predict TTI (s) and pkHRR (kW/m^2) values.

transparency and interpretability of machine learning models, revealing the influence of each feature on the model's output and thus making possible the development of more accurate and reliable prediction algorithms [30].

ChatGPT could recommend two different types of ML models for the prediction of our parameters: an ANN model enhanced with a K-Nearest Neighbors (K-NN) algorithm performing a local weighted regression (LWL), and a Gradient Boosted Trees (GBTs) model, which is a particular ensemble of decision tree. In the third stage, ANN and GBTs models are applied to the IPs dataset and trained by the data science software KNIME. To achieve the best overall performance, optimization methodologies were also carried out to properly tune the hyperparameters of the models based on the validation data. Finally, in the fourth stage, the predictions provided by the regression models were collected and compared with the actual values of multilayer's parameters (TTI and pkHRR), experimentally measured in laboratory (Sect. "Thermal and fire performances of the multilayer material").

By comparing the actual values with the predicted ones, the Mean Absolute Percentage Error (MAPE) of each model was evaluated to identify the one giving the best results. The estimation of MAPE for a regression model allows to quantify its effectiveness and reliability by Eq. 1, where N is the number of observations:

$$\text{MAPE}\ (\%) = 100 \times \frac{1}{N}\sum_{i=1}^{N}\frac{\left|\text{Actual value}_i - \text{Forecasted value}_i\right|}{\text{Actual value}_i} \tag{1}$$

MAPE is largely used in the field of regression analysis as percentage errors represent very intuitive indicators to understand model performances [54]. Table 1 displays an indicative outline to evaluate the goodness of a model based on the resulting MAPE value [55].

In view of the above, it is worth noticing that there is a strict interaction among the selected, designed, produced, and experimentally characterized multilayer material, ChatGPT, and the developed ML models. In fact, ChatGPT is fed by the input dataset, characterized by the presence of missing values, of

Table 1 Assessment and evaluation of prediction effectiveness by the interpretation of Mean Absolute Percentage Error (MAPE)

MAPE	Interpretation
< 10	Highly accurate forecasting
10–20	Good forecasting
20–50	Reasonable forecasting
> 50	Inaccurate forecasting

properties related to both the investigated multilayer and other materials that fall into the same class. The input dataset of properties is implemented by ChatGPT that finds suitable statistical indicators for completing the raw dataset. Once completed, the dataset is exploited for developing the ML models. Finally, the prediction of the parameters is compared with the actual values (i.e., those experimentally estimated).

Results and discussion

Manufacturing and chemical characterization of the multilayer material

The preparation of the multilayer material was designed based on the surface charge of the components at specific pH values so that the adhesion of PVP-silica blankets on the hemp rugs was promoted by electrostatic interaction. In the presence of charge-determining ions, the nature of a metal or metalloid (M) atom and the acidity of M-OH groups on the surface of inorganic nanoparticles directly influences their surface charge [56, 57]. The point of zero charge (PZC) represents the pH, at which the surface is not charged: therefore, at pH < PZC the surface is positively charged, whereas at pH > PZC it is negatively charged [56, 58]. As demonstrated in some previous works, the surface of the PVP-silica blanket is practically composed of silica, full of silanol groups [56, 58]. This finding is confirmed by the FTIR spectrum of PVP-silica (Figure S2), dominated by the intense vibrational band due to Si–O stretching at about 1090 cm^{-1}, with the bands at lower wavenumbers assigned to the stretching of Si–OH bonds (796 cm^{-1}) and the bending of Si–O-Si groups (584 cm^{-1}). As the PZC of silica is about 2.0, at pH 2.5 its surface is expected to exhibit a negative charge, while hemp should be characterized by a positive charge, having a PZC around 6 [59]. A bilayered sample (H-2PVP) was obtained by the deposition of one PVP-silica blanket on each side of the hemp blanket, as described in Sect. "Manufacturing of the multilayer material" and Fig. 1A.

Unlike PVP-silica alone, which achieved self-extinction [21], H-2PVP was not self-extinguishing during vertical flame spread test. For this reason, H-2PVP was further coated by 4 layers of PVP-silica blankets on each side to achieve self-extinction and V0 flammability class (see Sect. "Mechanical robustness and flammability behavior of the multilayer material"). Similarly to silica nanoparticles in the PVP fibers, commercial titanium oxide particles are rich in surface hydroxyl groups, as proved by the FTIR spectrum showed in Figure S2. Due to the different acidic characters of Si–OH and Ti–OH groups, the PZC of titanium dioxide is higher than that of silica (around 6) [57, 60, 61]. Therefore, at pH 5, the TiO_2 nanoparticles should be positively charged and thus encouraged to match the negatively charged silica particles and establish a cross-condensation. Owing to this straightforward manufacturing procedure, it is likely to expect strong interactions between the components of H-10PVP multilayer blanket, which appeared compact and uniform, as well as flexible (Fig. 1B).

The SEM images of H-10PVP (Fig. 1C) show the typical morphology of nonwoven electrospun fibers, with a multimodal diameter distribution, as previously reported [21, 57] and a rough surface revealing the embedded SiO_2 nanoparticles. The surface chemistry of the multilayer was investigated by ATR-FTIR spectroscopy and EDX analysis. The FTIR spectrum of H-10PVP confirms that hemp is thoroughly covered by the fiber mats, since it closely resembles that of bare mats (see Figure S2), showing the abovementioned bands due to silica and the bands between 1700 and 1300 cm^{-1} ascribed to PVP. The EDX elemental distribution, reported in the inset of Fig. 1C, agrees with the approximate composition of the hybrid fibers and reveals also the presence of TiO_2, which is hardly detectable by FTIR because of its low concentration.

To additionally prove the good adhesion of each layer in H-10PVP, the stability of PVP-silica blankets in a polar solvent, and the firm anchoring of titanium dioxide nanoparticles to the surface, the multilayer material underwent washing fastness tests. From the photograph, SEM image, and EDX data of the blankets after washing (Fig. 1D) it is possible to observe that the morphology and surface chemistry of the sample appear practically unmodified, as further confirmed by the FTIR spectrum (Fig. 1D), which is virtually

identical to that of the as-prepared sample. These results confirm the resistance of the multilayer material to repeated washing cycles.

Mechanical robustness and flammability behavior of the multilayer material

Unlike H-as10PVP which resembled wadding, H-10PVP exhibited notable mechanical strength and tensile response (see Sect. "Tensile behavior of the multilayer material"), stretchability, and structural compactness (see Fig. 1B). To prove these characteristics, H-10PVP (10 × 10 × 0.3 cm^3) was fixed at a metallic support and some glass marbles (total weight: 44.6 g) were placed on it. The sample did not break (Video 1), throughout the whole test, while H-as10PVP immediately lost its structural integrity after a few seconds (Video 2).

As previously mentioned, the procedure for the multilayer material preparation was continued up to the deposition of 5 double layers of PVP-silica because H-10PVP was found to exhibit V0 rate during vertical flame spread tests. More in detail, the sample (1.3 × 12.5 × 0.3 cm^3) captured the flame but this latter could not propagate along the sample, due to the formation of a ceramic and continuous carbonaceous residue, during the first combustion stages. Therefore, the flame immediately extinguished after its application, also resulting in the production of an almost inappreciable amount of smoke. Besides, it is worth mentioning that H-10PVP still showed its good mechanical behavior and structural compactness after the flammability test, which is likely due to the hemp layer remained practically undamaged after the flame exposure, thanks to the effective heat shielding effect exerted by the PVP-silica fibers (see Sect. "Mechanical robustness and flammability behavior of the multilayer material"). The negligible release of smoke and the absence of any dripping phenomena make this multilayer material a promising smoke suppressant textile, showing the consistency of the easily flammable and not classifiable (according to UL 94 vertical flame spread test) hemp rugs, in terms of mechanical strength, and the very low flammability of the nonwoven PVP-silica blankets. By using a configuration similar to that adopted for testing the mechanical strength of H-10PVP, the robustness of the multilayer material was also evaluated through the application of a gas lighter's flame to its surface, while the back side was sustaining a load (glass marbles of total weight = 44.6 g). Video 3 shows that H-10PVP does not capture the flame and the material preserves its structural integrity throughout the whole test, holding the load without any detrimental effect on its mechanical behavior. Besides, it is worth highlighting that after this test, H-10PVP also preserves its stretchability (Video 4) and mechanical strength, which means that the hemp layer probably undergoes only slight damage.

To investigate the burn-through resistance of the multilayer material, H-10PVP (10 × 10 × 0.3 cm^3 panel) was firmly fixed in vertical position (see Figure S1) and the flame of a butane gas blowpipe was directed perpendicular to the surface of the specimen, at an adequate distance to let the flame tip brush its middle. An IR camera was employed to record the back temperature (T_B) profile at the sample surface during the burn-through test. Burn-Through time (BTT) indicates the time, at which the material loses its structural integrity. It was possible to observe that during the flame application, an abundant amount of a white ceramic char forms, while the PVP layers undergo a fast decomposition (Video 5). As shown in Fig. 3A, H captures the flame after only 3 s (T_B = 140 °C), while H-10PVP requires around 21 s, revealing a very low surface flammability. Moving from the TTI point, the T_B of H-10PVP changes very slowly compared to that of H, probably due to the ceramic insulating char that slows down the heat exchange at the boundary layer and acts as a thermal barrier (Fig. 3B). Concerning H-10PVP, when the first PVP layers are fully degraded, the flaming combustion stops and the char starts its additional function of fire shield, protecting the underlying material, even at very high temperatures (> 600 °C). After almost 1 min (T_B = 705 °C) of flame application, H-10PVP still appears structurally intact. The flame does not burn through the sample: indeed, its back surface is free of holes and only marginally burned. Conversely, the hemp sample gives a BTT of around 18 s (T_B = 594 °C), which further underlines the low surface flammability and high burn-through resistance of H-10PVP.

Thermal and fire performances of the multilayer material

To investigate the thermal decomposition profile of the multilayer material, thermogravimetric analysis was performed under nitrogen and air atmosphere (Table 2). The same measurements were carried out

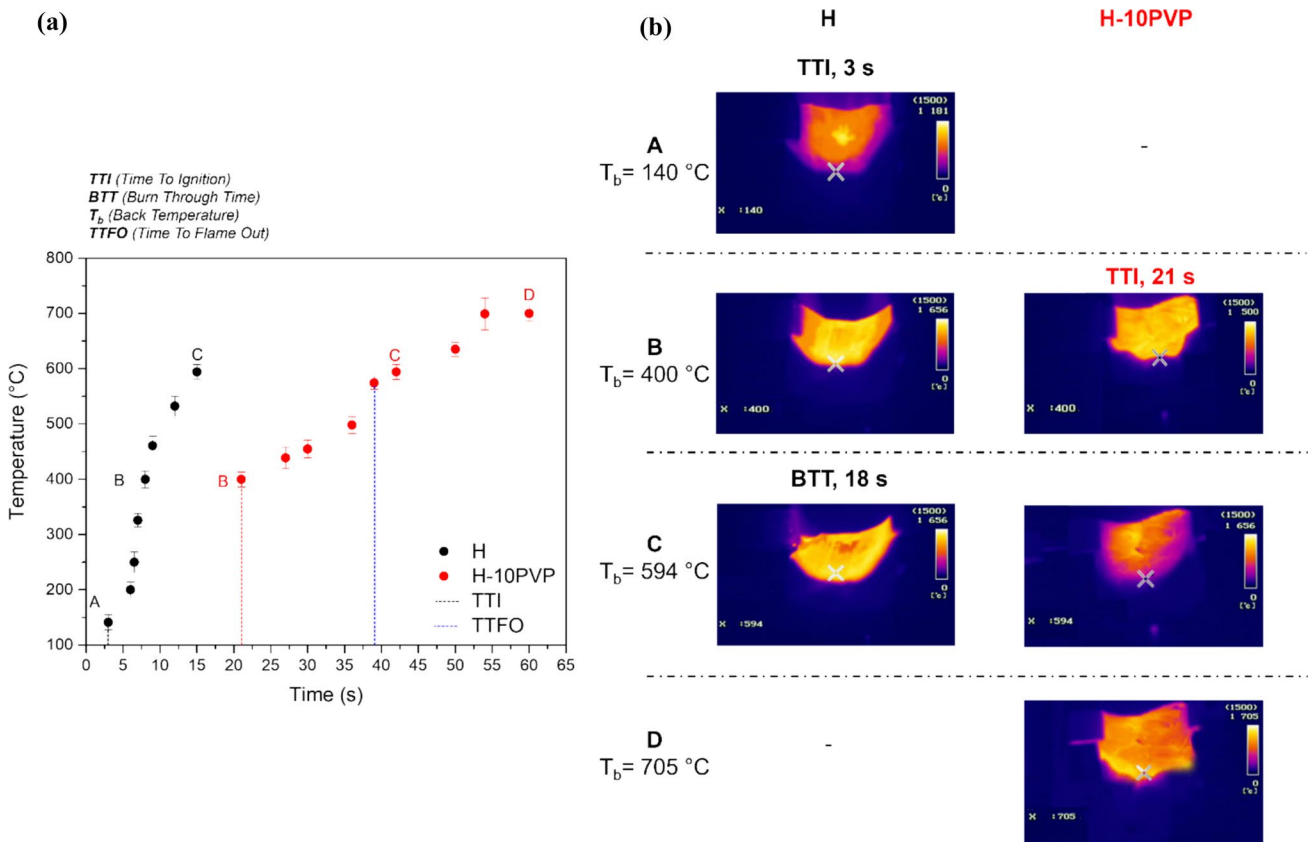


Figure 3 Results of the burn-through test on hemp and H-10PVP multilayer sample: **a** Back temperature of the sample as a function of time; **b** IR camera images taken at different times, with the indication of the TTI and BTT.

Table 2 Thermal data evaluated from TGA curves of all samples in N_2 and air. $T_{10\%}$ is the temperature, at which 10 wt.% loss is recorded. T_{max1} and T_{max2} are the temperatures, at which the weight loss rate reaches the maximum; the residues at T_{max1} and T_{max2}, and 800 °C are also reported

Sample	$T_{10\%}$ (°C)	T_{max1} (°C)	T_{max2} (°C)	Residue (wt.%) at		
				T_{max1}	T_{max2}	800 °C
Nitrogen						
PVP-silica	240	369	–	74	–	47
H	285	358	–	45	–	12
H-10PVP	303	340	–	69	–	34
Air						
PVP-silica	287	331	512	78	52	44
H	270	340	398	54	10	0
H-10PVP	247	362	572	76	56	45

on PVP-silica and hemp to study the main differences with H-10PVP. The presence of hemp in the multilayer materials results in a beneficial effect on the pyrolysis of H-10PVP, as it starts to decompose at higher $T_{10\%}$ compared to PVP-silica. On the other side, H-10PVP is also made of PVP-silica blankets, which are full of silica and titanium dioxide nanoparticles, both causing an anticipation of $T_{10\%}$ and a significant increase in the residual char at 800 °C, compared to hemp. Both the inorganic species show weak acidic characteristics promoting the dehydration of the polymer matrix and its charring behavior. Therefore, the ceramic char formed from the decomposition of H-10PVP, especially its first layers, lower the heat exchange at

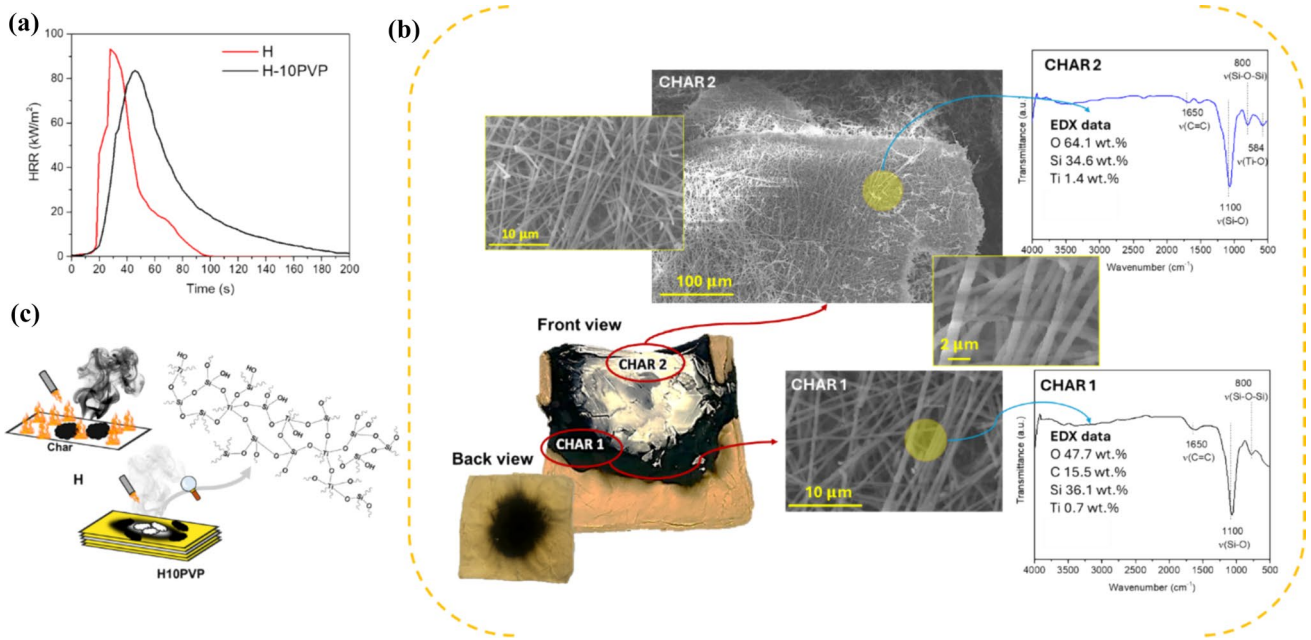


Figure 4 **a** Heat release rate (HRR) curves for hemp and H10-PVP from cone calorimetry tests; **b** SEM images, FTIR spectra and EDX elemental analysis data of char samples collected in two different spots of the H10-PVP after burn-through tests (CHAR 1 and CHAR 2); **C** Schematic representation of the flame retardant mechanism occurring in the multilayer material.

Table 3 Results from cone calorimetry tests for the investigated samples

Sample	TTI (s)	TTFO (s)	T HR (MJ/m^2)	ΔTHR (%)	HRR (kW/m^2)	ΔHRR (%)	pkHRR (kW/m^2)	Residue (wt.%)
H	18	47	2.2	–	15.7	–	98.2	1.1
H-10PVP	22	96	4.4	+50	23.1	+47	84.0	34.8

TTI = Time To Ignition, TTFO = Time To Flame Out, THR = Total Heat Release, HRR = Heat Release Rate, pkHRR = peak of Heat Release Rate

the boundary phase and act as thermal shield for the underlying material during the pyrolysis [21, 62]. In air atmosphere, the presence of acidic inorganic particles in H-10PVP leads to the lowest $T_{10\%}$; however, silica and titanium dioxide nanoparticles also boost the barrier effect of char toward the oxygen diffusion, shifting the main mass losses to higher temperatures and allowing for a residual mass at 800 °C comparable to that of PVP-silica, attesting a protective effect on the hemp substrate (Table 2).

Given the above, the combined use of PVP-silica blankets, titanium dioxide nanoparticles, and hemp in manufacturing the multilayer material concurs to obtain a product with good overall thermal stability.

To shed light on the flame retardant mechanisms taking place during the combustion of H-10PVP, its fire behavior was studied, in comparison to that of hemp alone, through forced-combustion tests by cone calorimetry. Figure 4A and Tables 3 and 4 show that the deposition of PVP-silica blankets on hemp completely changes its fire performance. The combustion of H-10PVP starts with the decomposition of

Table 4 Smoke parameters from cone calorimetry tests for the investigated samples

Sample	TSR (m^2/m^2)	ΔTSR (%)	SEA (m^2/kg)	ΔSEA (%)	CO/CO$_2$
H	33.3	–	233	–	0.06
H-10PVP	4.9	−85	37	−84	0.11

TSR = Total Smoke Release, SEA = Specific Extension Area

PVP, which is a well-known easily flammable polymer [21, 63], and it is followed by the formation of a ceramic layer that protects the underlying part of the sample from further degradation [64, 65]. Probably, the largest amount of hemp is allocated in this underlying part, which is only poorly influenced by the combustion process, due to the ceramic layer acting as an efficient barrier toward both heat and oxygen diffusion. Considering the multilayer material, silica nanoparticles compose the skeleton of PVP fibers, as demonstrated in a previous work [57], and its surface is characterized by the presence of titanium dioxide nanoparticles. Both these aspects account for an increase of the time to ignition of H-10PVP compared to the one of H (Table 3). In the case of H-10PVP, the release of combustible gases and heat propagation are significantly hindered by the inorganic species, which are intimately bonded to the polymer matrix. As shown in Fig. 4A and Table 3, during the combustion of the multilayer material, the heat is released over a longer time, which may be beneficial in all the applications where H-10PVP is employed as a passive fire protection component.

Unlike H, the combustion of H-10PVP causes the production of a huge amount of residual char (Table 3), likely ascribed to (1) the acidic characters of Si–OH and Ti–OH groups promoting the dehydration of the PVP matrix and its carbonatization, and (2) the formation of inorganic polymeric substructures, containing silicon- and titanium-based moieties, able to boost the thermal shielding action of the carbonaceous material [65, 66]. The peculiar chemical composition of H-10PVP allows for the occurrence of the above flame retardant mechanisms in both condensed and gas phases during the combustion, as also supported by the slight increase in CO/CO_2 (Table 4), which are responsible for the different flame retardant features of the multilayer material compared to hemp.

This flame retardant action enables H-10PVP to work as an outstanding smoke suppressant, as it shows a remarkable decrease of both TSR (85%) and SEA (84%), compared to H. The inorganic nanostructures do not affect only the time to ignition but also the total smoke release, as the inorganic polymeric substructures in the residual char contribute to reducing the release of combustible volatiles, the diffusion of oxygen, and the production of smoke gases (e.g., phenol, cresol, carbon dioxide, naphthalene, anthracene) during the combustion of the multilayer material [66].

To further investigate the phenomena taking place in the condensed phase, the residual char obtained from the combustion of H-10PVP, submitted to the flame of a small-scale butane burner (see Sect. "Thermal and fire performances of the multilayer material"), was deeply studied by ATR-FTIR and SEM–EDX analysis (Fig. 4B). Figure 4B gives a complete overview of the chemical compositions and morphologies related to different portions (CHAR 1 and CHAR 2) of char arising from the tested sample. Both CHAR 1 and CHAR 2 show the same functional groups of the unburned sample, also confirming a significant retention of silicon and titanium after the combustion. The amount of silicon and titanium progressively increases moving from CHAR 1 to CHAR 2, while the content of carbon strongly decreases, especially in comparison with the elemental composition of the unburned material. It is worth mentioning that the EDX analysis does not detect the presence of carbon in the case of CHAR 2 (Fig. 4B), as it forms in the region where the flame is applied during the burning test, causing the generation of a compact and continuous ceramic shield made of inorganic polymer substructures (i.e., Si–O-Ti moieties). From a morphological point of view, Fig. 4B provides clear evidence that the PVP-silica fibers are still present in CHAR 1 and CHAR 2, though the ones in CHAR 2 are most likely composed of inorganic polymers rising from cross-condensed substructures (Fig. 4C). This ceramic char looks so effective in protecting the underlying material that it is possible to observe some residual hemp with its characteristic texture: this finding may explain the good mechanical properties of H-10PVP, even during the application of a flame (see Sect. "Mechanical robustness and flammability behavior of the multilayer material"). Finally, the ATR-FTIR spectra of CHAR 1 and CHAR 2 reveal the appearance of a strong band at 1577 cm^{-1} related to the C = C stretching vibration highlighting a significant carbonization via dehydration of PVP matrix promoted by the acidic Si–OH and Ti–OH groups. All these results further confirm a strong flame retardant action in the condensed phase and shed some light on the features that enable this multilayer material to act as an effective smoke suppressant. It should be noted that these performances were achieved through the use of silica and titania nanoparticles, without any halogenated, epoxy, or aromatic components, i.e., potentially toxic and endocrine-disrupting compounds contained in many polymeric materials [67, 68]. Hence, in the disposal or recycling of the product at the end

of life, no harmful substances would be released into the environment. This multilayer material, obtained by a sustainable and simple route, represents a viable option to employ self-extinguishing nonwoven PVP fibers as fire protection component in combination with an easy flammable hemp-based product as reinforcement filler.

Tensile behavior of the multilayer material

To study the tensile response of hemp and to further support the mechanical robustness of the multilayer material (see Sect. "Mechanical robustness and flammability behavior of the multilayer material"), their stress–strain curves were collected (Figures S3 and S4). In agreement with previous works [69], after an initial stage of structural readjustment of the fabric meshes, the specimen stiffens for strains beyond 5%. This results in a steeper stress increase up to a maximum value of about 55 MPa, followed by failure of the fabric due to its further elongation that causes progressive tearing. The slope of the steepest section of the stress–strain curve, essentially representative of the specimen's stiffness, evaluated by a linear fitting, was approximately 600 MPa. Regarding the multilayer sample, the specimens appeared more delicate due to the presence of the electrospun PVP-silica nonwoven coating. Thus, special care was paid during the clamping of the specimens to avoid their premature damage, and the mechanical response was quite different. In particular, as clearly shown by the trend of the stress–strain curve presented in Figure S4, the tensile strength, again negligible for strains lower than 15%, shows a non-monotonic trend with a first increase up to about 2 MPa, followed by a partial yielding and a second increase until reaching a maximum stress of about 5.5 MPa. For further elongations, a noisy trend of the curve is observed, essentially due to a marked cleavage of the coating layers and tears in the internal fabric layer. In other words, the multilayer sample (H-10PVP) shows a mechanical response typical of materials that undergo delamination effects before catastrophic failure under load. Moreover, even in this case, it is possible to estimate the stiffness of layers of electrospun PVP and internal hemp fabric by evaluating the slopes of the two increasing stress sections (see fitting lines drawn in Figure S4). The results provided stiffness values approximately equal to 30 MPa and 50 MPa, respectively, i.e., one order of magnitude lower than the hemp fabric alone. This adverse effect, combined with a significant reduction in the maximum bearable stress, can be ascribed to the structural modifications undergone by the hemp fibres during the preparation phase of the multilayer sample and it is partly predictable given the enhanced wetting state of the hemp fabric resulting from the tested samples. However, these results from the tensile tests well agree with the qualitative observations concerning the mechanical robustness of the multilayer material (see Sect. "Mechanical robustness and flammability behavior of the multilayer material" and Video 1).

Prediction of time to ignition, total heat release and peak of heat release rate of the multilayer material

Application of the artificial neural network

Artificial neural networks (ANNs) are machine learning models largely employed for classification and regression in various application fields [31]. Like our brain, these networks are based on large collections of neurons linked by axons. In an artificial setup, neurons are replaced by neural units establishing connections to form a network. The strength of these connections can be either increased or decreased using a particular activation function, determining the neuron's output [31]. In a few words, ANNs represent complex nonlinear mathematical models able to convert a set of independent variables $x = (x_1, \ldots, x_n)$, referred to as network inputs into dependent variables $y = (y_1, \ldots, y_k)$, which are the network's outputs. The outcomes produced by the network are influenced by a collection of parameters $w = (w_1, \ldots, w_n)$, also known as weights. Equation 2 describes the way the network's outputs are derived from inputs:

$$y = f\left(\sum_j w_j * x_j + b\right) \tag{2}$$

where: x_j is the jth input, w_j is the jth weight, b is the bias, y is the output, and *f* is the activation function.

In the training stage of an ANN, neurons collect data and then store them in weights and biases to be used later in the prediction stage. The activation function, denoted as *f*, typically acts as a threshold function, triggering only the neurons matching the threshold criteria, and responsible for moving the signal to subsequent neurons. Sigmoid, nonlinear stepped, or

logistic functions are examples of activation functions. The training process involves an iterative procedure (i.e., backpropagation), which allows to appropriately adjust weights based on the input data. The final objective of this phase relies on finding the weight values able to reduce a specific error function. A backpropagation ANN algorithm may be optimized by different approaches, for example using the Bayesian regularization, which makes possible the development of a model with more efficient generalization capability [44]. An ANN is generally composed of three sections with varying numbers of neurons: one input layer, multiple hidden layers, and one output layer. Within these internal layers, the input signals are transmitted from the input to the output layer, as shown in Fig. 5A. One of the models developed in this research work is a fully connected feed-forward artificial neural network based on a multilayer perceptron. Particularly, two different feed-forward ANNs were implemented, one for each parameter to be predicted. The model's architecture and the layout of each layer are reported in Fig. 5B, showing both the ANNs. The structure mainly consists of one input layer with 15 variables, one hidden layer with 8 neurons (i.e., half plus one the neurons in the input layer), and one output layer with 1 neuron, returning the predicted parameter value of a specific textile material.

To predict the values of TTI and pkHRR for H-10PVP material, the networks perform a locally weighted regression through a K-NN algorithm. This supervised machine learning technique is used to weigh the training data based on their proximity to the new data, as each training data point receives a weight that is inversely related to its distance from the new data point (as shown in Figure S5). Therefore, during the regression process, the classifier prioritizes the local data (i.e., the training data within the K-regions closest to the new data), improving the accuracy of the predictions compared to the traditional regression methods [70].

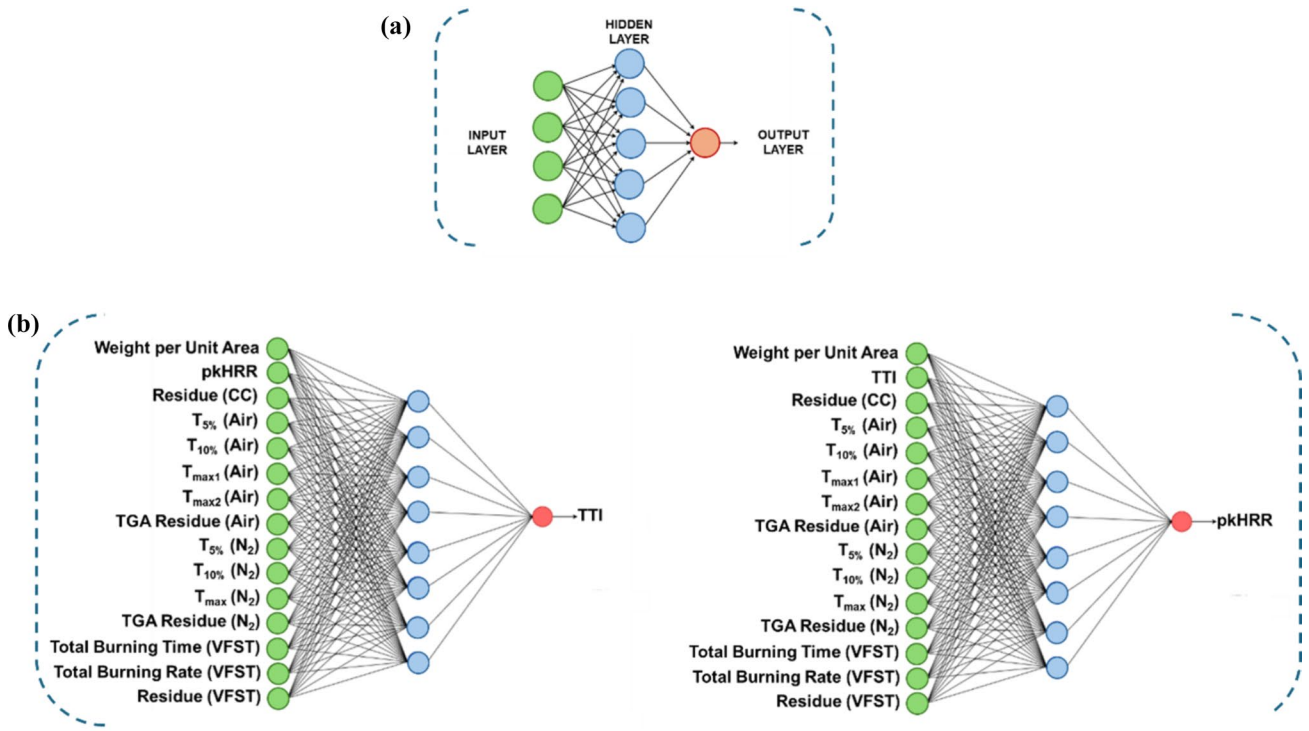


Figure 5 **a** Generic representation of an Artificial Neural Network (ANN) with three layers. **b** ANN models developed for the prediction of the TTI and pkHRR parameters. More in detail: weight per unit area was calculated as reported in Sect. "Experimental characterization", pkHRR is the peak of the heat release rate, residue (CC) is the residue from cone calorimetry tests, $T_{5\%}$ and $T_{10\%}$ are the temperatures, at which 5 wt.% and 10 wt.% losses in air (Air) and nitrogen (N_2) were recorded, T_{max1} and T_{max2} are the temperatures, at which the weight loss rate reached maximum, TGA residues indicate the residual masses at T > 600 °C, Total Burning Time (VFST) and Total Burning Rate (VFST) and the Residue (VFST) were measured during and after the vertical flame spread test (VFST), TTI is the time to ignition, THR is the total heat release.

In the training phase, MAPE was used as an indicator for the process related to the tuning of hyperparameters, providing the model's error for a particular combination. The minimization of this error involved the use of a "Parameter Optimization Loop (POL)" node. POL node was employed to find the best combination of hyperparameters (such as the "K" parameter of K-NN algorithm and the internal hyperparameters of the ANN), able to minimize the global error resulting from the application of locally weighted regression on each subset of the input dataset (extracted through the "X-Partitioner" node). We also used a hill-climbing search method to find the best combination of hyperparameters [71]. The following optimal values were found by this methodology:

- K = 3, learning rate equal to 0.001, momentum equal to 0.1 and number of epochs equal to 7300 for the prediction of TTI parameter;
- K = 2, learning rate equal to 0.005, momentum equal to 0.1 number of epochs equal to 8000 for the prediction of pkHRR parameter.

Then, the validation of the hyperparameters (the ones found using the optimization loop) was carried out by splitting the input data (Table S3) into two subsets: training set (Table S4, 70% of the input data) and validation set (Table S5, 30% of the input data). The validation dataset was used not only to perform the predictions but also to compare the predicted parameters with the actual values. The predicted values of TTI and pkHRR for H-10PVP sample from ANN models, applied on the whole input dataset (Table S3), are collected in Table 5, together with the MAPE values associated with the chosen hyperparameters. The predicted values were extracted through KNIME's "Numeric Scorer" node. More specifically, based on the validation data, MAPE was evaluated around 0.468 (≅ 47%) for the TTI parameter and 0.404 (≅ 40%) for the pkHRR parameter (as shown in Table 5), proving that our algorithms are characterized by a "reasonable" predictive capability (see Tables 1 and 5). The KNIME workflow employed in this research to implement the ANN models is presented in Figure S6.

APE values represent the errors measured on the test dataset and thus they are not comparable with the ones obtained from the validation dataset [54, 72]. This is especially true in cases where the test dataset consists of only one example. Therefore, although the APE values associated with the test dataset show very low and promising values, it is still necessary to consider the MAPE values evaluated on the validation dataset to have an idea about the true capability of the ANN models.

Application of decision trees and gradient-boosted trees

Among the machine learning tools, decision tree (DT) models represent a versatile and valuable methodology to address classification and regression challenges [73]. The architecture of these models mimics the process of human decision-making and thus decision trees break down a complex decision into a series of simple ones, facilitating the prediction of an output variable. A DT consists of nodes and branches forming a tree-like structure, where each node represents a "decision" based on certain input features and the branches represent the outcomes of these decisions [74]. The final predictions are the leaves of the tree and the nodes at the lowest level. The root of the tree begins with the whole input dataset, which is then split into subsets based on the values assumed by the parameters. The goal of each step along the decision tree is finding the best split, that is the one providing the highest variance reduction for a specific node, as a lower variance within nodes results in more accurate predictions. The splitting of the input dataset continues and creates a hierarchy of nodes and branches until the model meets some stopping criteria, such as

Table 5 Predicted values of TTI and PHHR for the multilayer material (H-10PVP) resulting from the application of ANN models on the input dataset. MAPE values are the model's errors, estimated on the validation data, quantifying the effectiveness and the reliability of models. APE values represent the model's errors, evaluated on the test data and associated with the chosen hyperparameters selected for the models

Parameter	Actual value	Predicted value	MAPE	APE
TTI (s)	22	19.12	0.468 (≅47%)	0.203 (≅19%)
pkHRR (kW/m^2)	84	118.189	0.404 (≅40%)	0.299 (≅17%)

a maximum depth of the tree or a minimum number of samples per leaf. In regression problems, decision trees (also called "regression trees") predict numerical values by segmenting the "input space" into distinct regions, where the prediction for each leaf is typically determined by the average outcome of the training instances within that region [75]. Figure 6 shows the typical structure of a DT (Fig. 6A) and its capability to separate the input space into different regions (Fig. 6B).

Moreover, the working process of DTs inherently makes this machine learning tool particularly indicated for handling missing values, which is a common issue in real-world input datasets. This peculiar feature of DTs allows to manage missing data without requiring extensive preprocessing or replacing strategies. This aspect is significantly advantageous, as the integrity and the statistical distribution of the original input dataset are preserved. Gradient Boosted Trees (GBTs) enhance the predictive performance of DTs by combining the results of multiple DTs models. More in detail, the application of GBTs on an input dataset leads to an ensemble, as each decision tree focuses on reducing the error made by its predecessor, hence improving the overall model's performance. GBTs methodology has proven its effectiveness in machine learning challenges where the implementation of a single DT cannot provide a satisfactory level of predictiveness [76]. GBTs are based on an optimization algorithm, named "Gradient Descent", involving the minimization of a loss function, which quantifies the difference between the predicted and actual outcomes at each iteration [77]. The residual values of several iteration steps represent the training dataset of a next tree. This latter tries to fix the error (i.e., the difference between the prediction of a current tree and the actual target value) made by the previous one through the prediction of its error. This iteration process allows for improving the model's predictiveness, as the trees learn by doing (see Fig. 7).

The gradient descent process aims to get as close as possible to the minimum of the loss function and it repeats for a number of iterations until the error is no longer significantly reduced. The gradient refers to the direction where the next tree lowers the total prediction error based on the previous predictions and the gradient of the loss function. In other words, for a given loss function L(y, F(x)), where x is the given input, y is the actual outcome value and F(x) is the predicted value given the input x, the loss function quantifies how far off our predictions are from the actual values. In regression tasks, common choices for the L function are represented by mean squared error and MAPE. The gradient of the loss function points toward the direction where the loss function increases more sharply. The gradient is considered

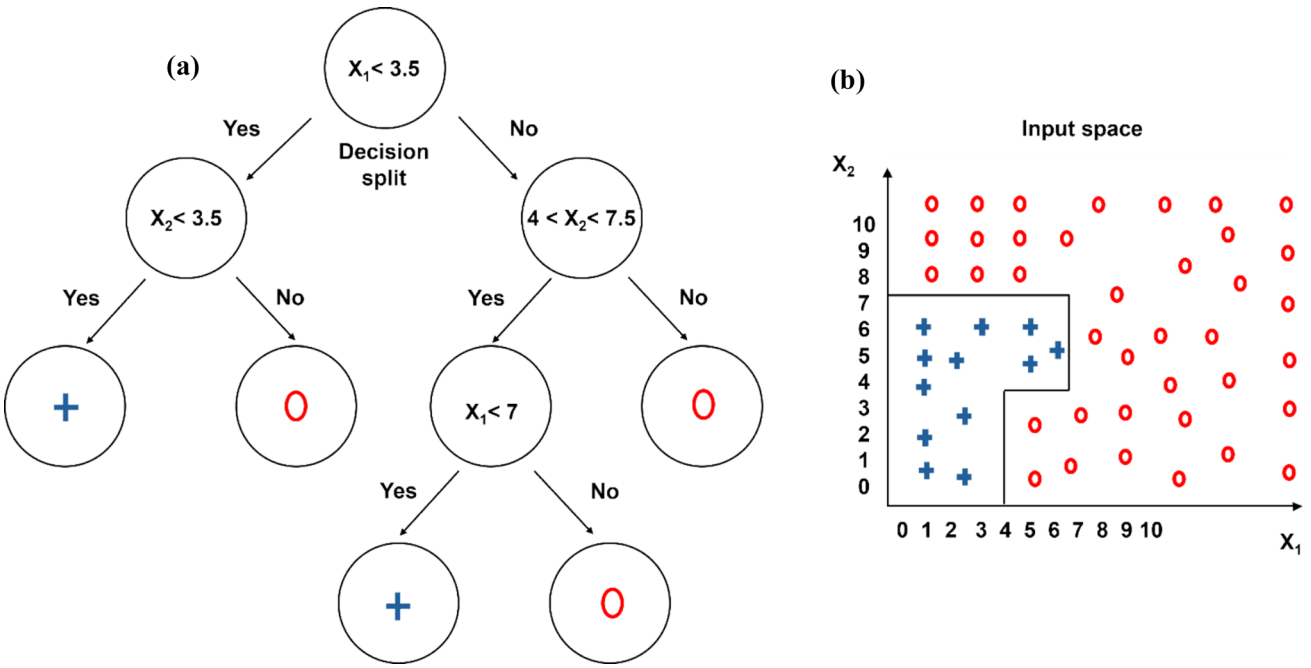


Figure 6 **a** An example of decision tree and **b** the resulting input space subdivision.

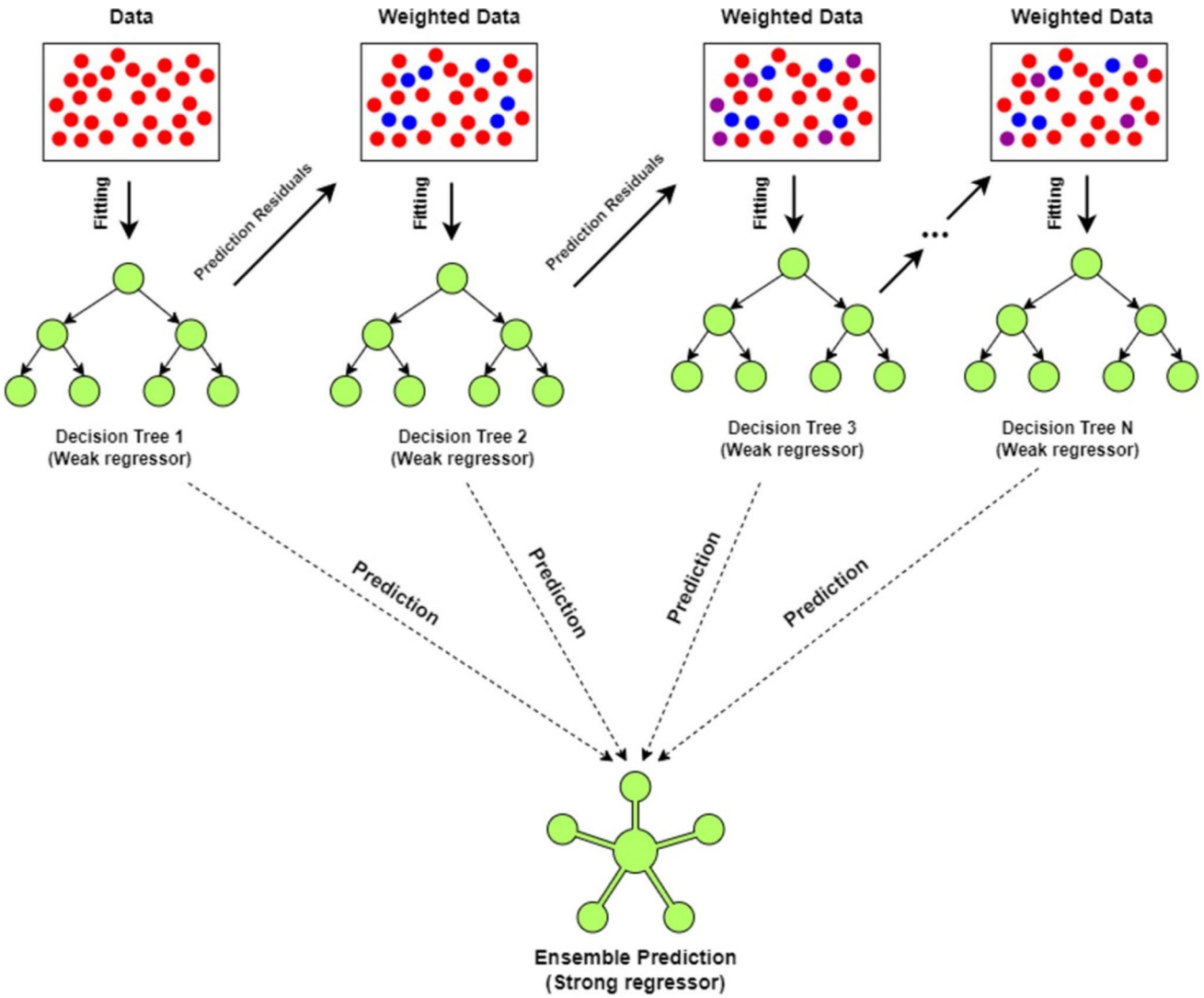


Figure 7 The building process of Gradient Boosted Trees (GBTs), starting from an input dataset.

with a negative sign, as the minimization of the loss occurs in the opposite direction of the gradient. For a given set of predictions F(x), the gradient of the loss function with respect to these predictions at each point x_i is calculated as shown in Eq. 3:

$$g_i = \frac{\partial L_i\left(y_i, F\left(x_i\right)\right)}{\partial F\left(x_i\right)} \tag{3}$$

The equation gives back how to adjust the predictions $F\left(x_i\right)$ to decrease the loss for each instance i. The size of the steps taken in the gradient descent process is controlled by a parameter known as "learning rate", which balances the speed of learning against the risk of overfitting (i.e., the model overly adapts to the training data and then fails on new data). The gradient descent algorithm is graphically shown in Figure S7.

As for the ANN models, we trained two separated GBTs models (one for each parameter to be predicted, i.e., TTI and pkHRR) and measured the error using MAPE as an indicator. To compare the outcomes resulting from the two types of models (ANN and GBTs), the tuning of the hyperparameters was performed by employing the same procedure followed in the case of the ANNs (see Sect. "Application of the artificial neural network"). Also, the same training dataset and validation dataset (see Tables S4 and S5) were considered for the application of GBTs models. The hyperparameters of GBTs models are represented by the number of trees, related to the ensemble, and

the learning rate. The optimal values found for the hyperparameters from the parameter optimization loop are (1) the number of trees equal to 400 and (2) the learning rate equal to 0.001, for the prediction of both parameters. By using the whole input dataset (see Table S3), the implementation of GBTs models on validation data gives the predicted values (extracted through KNIME's "Numeric Scorer" node) of TTI and pkHRR for H-10PVP sample listed in Table 6. MAPE values, calculated on the validation data, are 0.431 (≅ 43%) and 0.336 (≅ 34%), respectively for the TTI parameter and the pkHRR parameter. The lower MAPE values compared to those resulting from the application of ANNs prove that GBTs models are the best choice for the prediction of TTI and pkHRR belonging to the considered textile materials. Also, the lower MAPE values (see Tables 1, 5, and 6) additionally confirm that decision trees generally perform better and are more reliable than ANNs, when the input datasets contain missing values. The KNIME workflow employed in this research to implement the GBTs models is reported in Figure S8.

Overall, decisional trees significantly differ from ANNs. As above mentioned, ANNs are composed of different interconnected layers of neurons making the prediction, while decisional trees are tree-like structures with nodes representing the decisions. The main difference between the two models is the learning approach. Indeed, ANNs learn pattern through weight and biases adjusted by backpropagation, while the decision trees split the data on the basis feature conditions to create branches. There are no possibilities to identify, from the very beginning, the best performing ML model. Indeed, as it shines through this research work, the only possible way relies on the development of the models and on the comparison of the predicted data with the experimentally measured values (actual values). Besides, there are other parameters that may impact on the quality of the ML model, namely the completeness of the database, its statistical significance and reliability, and the type of input parameters, among others. In the present work, based on the given boundary conditions (see Sect. "Machine learning modelling and design strategy"), decisional trees must be preferred to ANNs, as they provide the lowest values of model's errors (MAPE and APE, Tables 5 and 6) and computational expense.

Conclusions

To overcome the poor mechanical behavior of electrospun-based materials and to widen their application in advanced sectors, in this research work, we manufactured a multilayer material (MM) based on thermally treated PVP-silica based electrospun fibers, TiO_2 nanoparticles, and hemp, exploiting surface charge interactions. An intensive washing in water of MM did not affect its surface chemistry, morphology, and layer adhesion. Unlike electrospun PVP-silica blankets, MM showed high stretchability, satisfactory tensile behavior, also carrying a load during the application of a direct flame and showing an acceptable mechanical behavior, as assessed through tensile tests. Compared to the easily flammable hemp, the designed multilayer material exhibited V0 class in the UL 94 vertical burning tests, as well as slightly higher ignition time, and 85% lower total smoke release in forced-combustion tests. The combustion of the MM resulted in the formation of a ceramic and coherent residual char, slowing down the diffusion of smoke gases and exerting a hybrid flame retardant action in both condensed and gas phases. Besides, this char acted as an excellent fire shield, as it appeared impenetrable to the blowpipe flame applied during the burn-through test of MM.

Finally, an artificial neural network was tested to predict two important cone calorimetry parameters, i.e., the Time to Ignition and peak of Heat Release Rate, based on a dataset of physical, thermal, and fire parameters of treated textiles. We demonstrated

Table 6 Predicted values of TTI and pkHHR for the multilayer material (H-10PVP) resulting from the application of GBTs models on the input dataset. MAPE values are the model's errors, estimated on the validation data, quantifying the effectiveness and the reliability of models. APE values represent the model's errors, evaluated on the test data and associated with the chosen hyperparameters selected for the models

Parameter	Actual value	Predicted value	MAPE	APE
TTI (s)	22	19.986	0.431 (≅43%)	0.277 (≅28%)
pkHRR (kW/m^2)	84	78.307	0.336 (≅34%)	0.158 (≅16%)

that the integration of ChatGPT to perform a data enhancement and the implementation of well-designed machine learning models, featuring Gradient Boosted Trees, allow for a prediction with satisfactory accuracy, evaluated by Absolute Percentage Errors, even in case of some missing input data. The results of this research may pave the way for the design of more sustainable flame retarded functional multilayer materials based on electrospun polymers and natural fibers, and the use of reliable AI-assisted models that allow for the prediction of materials parameters, hence saving time and experimental efforts.

Acknowledgements

Dr. Aurelio Bifulco acknowledges the Italian Ministry of Education and Research, PON R&I 2014-2020—Asse IV "Istruzione e ricerca per il recupero—REACT-EU"—Azione IV.6—"Contratti di ricerca su tematiche Green", for the financial support concerning his employment contract. The AI-TRANSPWOOD project, HORIZON-CL4-2023-RESILIENCE-01-23 (Grant Agreement 101138191), is gratefully acknowledged. This project is co-founded by the European Union. Views and opinions expressed are however those of the authors only and do not necessarily reflect those of the European Union or HaDEA. Neither the European Union nor the granting authority can be held responsible for them.

Author contributions

Aurelio Bifulco: Conceptualization, Investigation, Formal analysis, Validation, Supervision, Writing—Original Draft. Immacolata Climaco: Investigation, Formal analysis, Methodology, Writing—Original Draft. Angelo Casciello: Conceptualization, Investigation, Formal analysis, Methodology, Writing—Original Draft. Jessica Passaro: Investigation, Formal analysis, Methodology. Daniele Battegazzore: Investigation, Formal analysis. Viviana Nebbioso: Investigation, Formal analysis. Pietro Russo: Methodology, Investigation, Formal analysis, Writing—Review and Editing. Claudio Imparato: Formal analysis, Investigation, Writing—Original Draft. Antonio Aronne: Validation, Supervision, Writing—Review and Editing. Giulio Malucelli: Conceptualization, Methodology, Validation, Supervision, Writing—Review and Editing.

Data availability

Data will be made available on request.

Declarations

Conflict of interest Aurelio Bifulco reports financial support was provided by Italian Ministry of Education and Research. Aurelio Bifulco reports a relationship with University of Naples Federico II that includes: employment. If there are other authors, they declare that they have no known competing financial interests or personal relationships that could have appeared to influence the work reported in this paper.

Supplementary Information The online version contains supplementary material available at https://doi.org/10.1007/s10853-024-10529-3.

Open Access This article is licensed under a Creative Commons Attribution-NonCommercial-NoDerivatives 4.0 International License, which permits any non-commercial use, sharing, distribution and reproduction in any medium or format, as long as you give appropriate credit to the original author(s) and the source, provide a link to the Creative Commons licence, and indicate if you modified the licensed material. You do not have permission under this licence to share adapted material derived from this article or parts of it. The images or other third party material in this article are included in the article's Creative Commons licence, unless indicated otherwise in a credit line to the material. If material is not included in the article's Creative Commons licence and your intended use is not permitted by statutory regulation or exceeds the permitted use, you will need to obtain permission directly from the copyright holder. To view a copy of this licence, visit http://creativecommons.org/licenses/by-nc-nd/4.0/.

References

[1] Agarwal S, Greiner A, Wendorff JH (2013) Functional materials by electrospinning of polymers. Prog Polym Sci 38:963–991

[2] Teo WE, Ramakrishna S (2006) A review on electrospinning design and nanofibre assemblies. Nanotechnology 17:R89

[3] Agarwal S, Wendorff JH, Greiner A (2008) Use of electrospinning technique for biomedical applications. Polymer (Guildf) 49:5603–5621

[4] Sill TJ, Von Recum HA (2008) Electrospinning: applications in drug delivery and tissue engineering. Biomaterials 29:1989–2006

[5] Lv D, Zhu M, Jiang Z et al (2018) Green electrospun nanofibers and their application in air filtration. Macromol Mater Eng 303:1800336

[6] Chen Y, Sui L, Fang H et al (2019) Superior mechanical enhancement of epoxy composites reinforced by polyimide nanofibers via a vacuum-assisted hot-pressing. Compos Sci Technol 174:20–26

[7] Huang L, Liao R, Bu N et al (2024) Electrospun konjac glucomannan/polyvinyl alcohol long polymeric filaments incorporated with tea polyphenols for food preservations. Foods 13:284

[8] Gallo E, Fan Z, Schartel B, Greiner A (2011) Electrospun nanofiber mats coating—new route to flame retardancy. Polym Adv Technol 22:1205–1210

[9] Torres-Martínez EJ, Vera-Graziano R, Cervantes-Uc JM, Bogdanchikova N, Olivas-Sarabia A, Valdez-Castro R, Serrano-Medina A, Iglesias AL, Pérez-González GL, Cornejo-Bravo JM, Villarreal-Gómez LJ (2020) Preparation and characterization of electrospun fibrous scaffolds of either PVA or PVP for fast release of sildenafil citrate. E-Polymers 20(1):746–758

[10] Khaleel MR, Hashim FS, Alkhayatt AHO (2024) Preparation, characterization, and the antimicrobial activity of PVA-PVP/ZnO nanofiber films via indigenous electrospinning setup. J Mol Struct 1310:138325

[11] Fan JT, Weerheijm J, Sluys LJ (2015) Glass interface effect on high-strain-rate tensile response of a soft polyurethane elastomeric polymer material. Compos Sci Technol 118:55–62

[12] Fan JT, Weerheijm J, Sluys LJ (2016) Compressive response of a glass–polymer system at various strain rates. Mech Mater 95:49–59

[13] Fan JT, Weerheijm J, Sluys LJ (2016) Compressive response of multiple-particles-polymer systems at various strain rates. Polymer (Guildf) 91:62–73

[14] Bhardwaj N, Kundu SC (2010) Electrospinning: a fascinating fiber fabrication technique. Biotechnol Adv 28:325–347

[15] Loría-Bastarrachea MI, Herrera-Kao W, Cauich-Rodríguez JV et al (2011) A TG/FTIR study on the thermal degradation of poly (vinyl pyrrolidone). J Therm Anal Calorim 104:737–742

[16] Gao D, Xin B, Newton MAA (2023) Preparation and characterization of electrospun PVDF/PVP/SiO_2 nanofiber membrane for oil-water separation. Colloids Surf A Physicochem Eng Asp 676:132153

[17] Rahmanian V, Pirzada T, Barbieri E et al (2023) Mechanically robust, thermally insulating and photo-responsive aerogels designed from sol-gel electrospun PVP-TiO_2 nanofibers. Appl Mater Today 32:101784

[18] Kim G, Doh SJ, Kim Y et al (2022) Electrospun polyvinyl alcohol composite nonwovens for air filtration materials in the humidity environment. Fibers Polym 23:690–698

[19] Giannella V, Branda F, Passaro J et al (2020) Acoustic improvements of aircraft headrests based on electrospun mats evaluated through boundary element method. Appl Sci 10:5712

[20] Newsome TE, Olesik SV (2014) Electrospinning silica/polyvinylpyrrolidone composite nanofibers. J Appl Polym Sci 131:21

[21] Passaro J, Russo P, Bifulco A et al (2019) Water resistant self-extinguishing low frequency soundproofing polyvinylpyrrolidone based electrospun blankets. Polymers (Basel) 11:1205

[22] Guadagno L, Raimondo M, Vittoria V et al (2014) Development of epoxy mixtures for application in aeronautics and aerospace. Rsc Adv 4:15474–15488

[23] Bifulco A, Imparato C, Aronne A, Malucelli G (2022) Flame retarded polymer systems based on the sol-gel approach: Recent advances and future perspectives. J Sol-Gel Sci Technol 1–25

[24] Gonzalez V, Lou X, Chi T (2023) Evaluating environmental impact of natural and synthetic fibers: a life cycle assessment approach. Sustainability 15:7670

[25] Khanal A, Shah A (2024) Techno-economic analysis of hemp production, logistics and processing in the US. Biomass 4:164–179

[26] Ao X, Vázquez-López A, Mocerino D et al (2023) Flame retardancy and fire mechanical properties for natural fiber/polymer composite: a review. Compos Part B Eng 268:111069

[27] Qi P, Chen F, Li Y et al (2023) A review of durable flame-retardant fabrics by finishing: fabrication strategies and challenges. Adv Fiber Mater 5:731–763

[28] Kundu CK, Li Z, Song L, Hu Y (2020) An overview of fire retardant treatments for synthetic textiles: from traditional approaches to recent applications. Eur Polym J 137:109911
[29] Sadan MK, Ahn H-J, Chauhan GS, Reddy NS (2016) Quantitative estimation of poly (methyl methacrylate) nano-fiber membrane diameter by artificial neural networks. Eur Polym J 74:91–100
[30] Uddin MJ, Fan J (2024) Interpretable machine learning framework to predict the glass transition temperature of polymers. Polymers (Basel) 16:1049
[31] Ciaburro G, Iannace G, Passaro J et al (2020) Artificial neural network-based models for predicting the sound absorption coefficient of electrospun poly (vinyl pyrrolidone)/silica composite. Appl Acoust 169:107472
[32] Amor N, Noman MT, Petru M et al (2024) Design and optimization of machinability of ZnO embedded-glass fiber reinforced polymer composites with a modified white shark optimizer. Expert Syst Appl 237:121474
[33] Liu Y, Van der Meer FP, Sluys LJ, Fan JT (2020) A numerical homogenization scheme used for derivation of a homogenized viscoelastic-viscoplastic model for the transverse response of fiber-reinforced polymer composites. Compos Struct 252:112690
[34] Pomázi Á, Toldy A (2023) Predicting the flammability of epoxy resins from their structure and small-scale test results using an artificial neural network model. J Therm Anal Calorim 148:243–256
[35] Parandekar PV, Browning AR, Prakash O (2015) Modeling the flammability characteristics of polymers using quantitative structure–property relationships (QSPR). Polym Eng Sci 55:1553–1559
[36] Asante-Okyere S, Xu Q, Mensah RA et al (2018) Generalized regression and feed forward back propagation neural networks in modelling flammability characteristics of polymethyl methacrylate (PMMA). Thermochim Acta 667:79–92
[37] Jiang L, Mensah RA, Asante-Okyere S et al (2022) Developing an artificial intelligent model for predicting combustion and flammability properties. Fire Mater 46:830–842
[38] Ye S, Li B, Li Q et al (2019) Deep neural network method for predicting the mechanical properties of composites. Appl Phys Lett 115:16
[39] Ansari N, Babaei V, Najafpour MM (2024) Enhancing catalysis studies with chat generative pre-trained transformer (ChatGPT): conversation with ChatGPT. Dalt Trans 53:3534–3547
[40] Yenduri G, Ramalingam M, Selvi GC et al (2024) Gpt (generative pre-trained transformer)–a comprehensive review on enabling technologies, potential applications, emerging challenges, and future directions. IEEE Access 12:54608–54649
[41] Luu RK, Arevalo S, Lu W, et al (2024) Learning from Nature to Achieve Material Sustainability: Generative AI for Rigorous Bio-inspired Materials Design. An MIT Exploration of Generative AI. https://doi.org/10.21428/e4baedd9.33bd7449
[42] Bifulco A, Casciello A, Imparato C et al (2023) A machine learning tool for future prediction of heat release capacity of in-situ flame retardant hybrid $Mg(OH)_2$-Epoxy nanocomposites. Polym Test 127:108175
[43] Amor N, Noman MT, Petru M et al (2021) Neural network-crow search model for the prediction of functional properties of nano TiO_2 coated cotton composites. Sci Rep 11:13649
[44] Amor N, Noman MT, Ismail A et al (2022) Use of an artificial neural network for tensile strength prediction of nano titanium dioxide coated cotton. Polymers (Basel) 14:937
[45] Passaro J, Bifulco A, Calabrese E et al (2023) Hybrid hemp particles as functional fillers for the manufacturing of hydrophobic and anti-icing epoxy composite coatings. ACS Omega 8:23596–23606
[46] Branda F, Malucelli G, Durante M et al (2016) Silica treatments: a fire retardant strategy for hemp fabric/epoxy composites. Polymers (Basel) 8:313
[47] Cheng X-W, Guan J-P, Chen G et al (2016) Adsorption and flame retardant properties of bio-based phytic acid on wool fabric. Polymers (Basel) 8:122
[48] Bifulco A, Imparato C, Climaco I et al (2024) Multifunctional fire-resistant and flame-triggered shape memory epoxy nanocomposites containing carbon dots. Chem Eng J 484:149327
[49] Ureel Y, Vermeire FH, Sabbe MK, Van Geem KM (2023) Beyond group additivity: transfer learning for molecular thermochemistry prediction. Chem Eng J 472:144874
[50] Ghosh MK, Elliott SN, Somers KP et al (2023) Group additivity values for entropy and heat capacities of C2–C8 alkanes, alkyl hydroperoxides, and their radicals. Combust Flame 257:112706
[51] Emmanuel T, Maupong T, Mpoeleng D et al (2021) A survey on missing data in machine learning. J Big Data 8:140
[52] Fillbrunn A, Dietz C, Pfeuffer J et al (2017) KNIME for reproducible cross-domain analysis of life science data. J Biotechnol 261:149–156
[53] Trovato V, Sfameni S, Ben Debabis R et al (2023) How to address flame-retardant technology on cotton fabrics by using functional inorganic sol-gel precursors and nanofillers: flammability insights, research advances, and sustainability challenges. Inorganics 11:306

[54] de Myttenaere A, Golden B, Le Grand B, Rossi F (2016) Mean absolute percentage error for regression models. Neurocomputing 192:38–48
[55] Moreno JJM, Pol AP, Abad AS, Blasco BC (2013) Using the R-MAPE index as a resistant measure of forecast accuracy. Psicothema 25:500–506
[56] Chen D, Zhao X, Jing X et al (2023) Bio-inspired functionalization of electrospun nanofibers with anti-biofouling property for efficient uranium extraction from seawater. Chem Eng J 465:142844
[57] Passaro J, Imparato C, Parida D et al (2022) Electrospinning of PVP-based ternary composites containing SiO_2 nanoparticles and hybrid TiO_2 microparticles with adsorbed superoxide radicals. Compos Part B Eng 238:109874
[58] Prorokova NP, Odintsova OI, Rumyantseva VE et al (2023) Giving improved and new properties to fibrous materials by surface modification. Coatings 13:139
[59] Akköz Y, Coşkun R (2023) Preparation of highly effective bio-adsorbent from hemp fiber for removal of malachite green oxalate (MGO). Cellulose 30:4511–4525
[60] Xie Z, Meng Q, Hu Y et al (2024) Amorphous titanium dioxide with abundant defects induced by incorporation of silicon dioxide: a potential non-radical activator of hydrogen peroxide. J Colloid Interface Sci 653:1006–1017
[61] Piasecki W, Lament K (2024) Application of potentiometric and electrophoretic measurements to evaluate the reversibility of adsorption of divalent ions from a solution on titanium dioxide. Molecules 29:555
[62] Zhuo T, Xin B, Chen Z et al (2021) Enhanced thermal insulation properties of PI nanofiber membranes achieved by doping with SiO_2 nanoparticles. Eur Polym J 153:110489
[63] Cao X, Chen D, Tiwari SK et al (2024) Implanting MOF Co-doped carbon nanotubes into PVP as flame-retardant to fabricate high performance PVA/SA aerogel nanocomposites. J Environ Chem Eng 12:111977
[64] Hu G, Zhang X, Bu M, Lei C (2022) Toughening and strengthening epoxy resins with a new bi-DOPO biphenyl reactive flame retardant. Eur Polym J 178:111488
[65] Venezia V, Matta S, Lehner S et al (2021) Detailed thermal, fire, and mechanical study of silicon-modified epoxy resin containing humic acid and other additives. ACS Appl Polym Mater 3:5969–5981
[66] Bifulco A, Marotta A, Passaro J et al (2020) Thermal and fire behavior of a bio-based epoxy/silica hybrid cured with methyl nadic anhydride. Polymers (Basel) 12:1661
[67] Rex KR, Chandra S, Pavithra K, et al (2024) Chemistry, production, and consumption of industrial endocrine disrupting chemicals. In: Endocrine-Disrupting Chemicals. Elsevier, pp 17–46
[68] Metcalfe CD, Bayen S, Desrosiers M et al (2022) An introduction to the sources, fate, occurrence and effects of endocrine disrupting chemicals released into the environment. Environ Res 207:112658
[69] Misnon MI, Islam MM, Epaarachchi JA, Lau KT (2015) Analyses of woven hemp fabric characteristics for composite reinforcement. Mater Des 66:82–92
[70] Cleveland WS, Devlin SJ (1988) Locally weighted regression: an approach to regression analysis by local fitting. J Am Stat Assoc 83:596–610
[71] Plähn JAN (2022) A Prototype Quest Generator for Simulating Human-Authored Narrative, Master thesis, Chalmers University of Technology, https://hdl.handle.net/2077/74248.
[72] Cullen E, Johnson T (2023) The Impact of Artificial Intelligence on Materials Engineering Research, Major Qualifying Project, Worcester Polytechnic Institute, https://digital.wpi.edu/downloads/6108vg03d
[73] Navada A, Ansari AN, Patil S, Sonkamble BA (2011) Overview of use of decision tree algorithms in machine learning. In: 2011 IEEE Control and System Graduate Research Colloquium. pp 37–42
[74] Rokach L, Maimon O (2005) Decision trees BT—data mining and knowledge discovery handbook. In: Maimon O, Rokach L (eds). Springer US, Boston, MA, pp 165–192
[75] Loh W-Y (2011) Classification and regression trees. WIREs Data Min Knowl Discov 1:14–23
[76] Dev VA, Eden MR (2019) Gradient Boosted Decision Trees for Lithology Classification. In: Muñoz SG, Laird CD, Realff MJBT-CACE (eds) Proceedings of the 9 International Conference on Foundations of Computer-Aided Process Design. Elsevier, pp 113–118
[77] Haji SH, Abdulazeez AM (2021) Comparison of optimization techniques based on gradient descent algorithm: a review. PalArch's J Archaeol Egypt/Egyptol 18:2715–2743

Publisher's Note Springer Nature remains neutral with regard to jurisdictional claims in published maps and institutional affiliations.